Mechanical Properties and Superstructure of Poly(ethylene terephthalate) Fibers Zone-Drawn and Zone-Annealed by CO_2 Laser Heating

AKIHIRO SUZUKI, NORIAKI MOCHIDUKI

Department of Applied Chemistry and Biotechnology, Faculty of Engineering, Yamanashi University, 4-3-11 Takeda, Kofu 400-8511, Japan

Received 13 December 2000; accepted 13 March 2001

ABSTRACT: A laser-heating zone-drawing and zone-annealing method using a continuous-wave carbon dioxide laser was applied to poly(ethylene terephthalate) (PET) fiber to improve its mechanical properties. The as-spun fiber was zone-drawn under a applied tension (σ_a) of 4.44 MPa at a laser power density (PD) of 6.08 W cm^{-2}, and then the laser-heated zone-drawn fiber was zone-annealed. The laser-heating zone-annealing was carried out in three steps: the first annealing was carried out under σ_a = 139 MPa at 4.83 W cm^{-2}; the second annealing was carried out under σ_a = 283 MPa at 4.83 W cm^{-2}, and the third annealing was carried out under σ_a = 432 MPa at 3.45 W cm^{-2}. The surface temperature distribution of the fiber irradiated with the CO_2 laser was measured by using an infrared thermographic camera equipped with a magnifying lens. The relation between the laser power and the surface temperature of the fiber became clear in the laser-heating zone-drawing and the laser-heating zone-annealing. The fiber obtained finally had a birefringence of 0.239, a degree of crystallinity of 55%, a tensile modulus of 19.8 GPa, and a storage modulus of 25.7 GPa at 25°C. In FTIR measurements, a *trans* conformation increased with the processing, but a *gauche* one decreased. The laser-heating zone-drawing and zone-annealing method was found to be effective in producing the PET fiber with high modulus and high strength. J Appl Polym Sci 82: 2775–2783, 2001

Key words: PET fiber; CO_2 laser-heating; zone-drawing/zone-annealing; mechanical properties; superstructure

INTRODUCTION

A carbon dioxide (CO_2) laser was applied to welding, cutting, and cladding for ceramics and metals, annealing of semiconductor, and improvement of the surface properties of carbon or other ceramic fibers.[1–6] A wide variety of application is possible in material processing. However, the CO_2 laser is hardly applied to polymers, and there is very little literature in this field: etching of polymer[7] and curing of epoxy resin.[8]

We have so far applied a zone-heater to the drawing and annealing for various polymers and then published articles on the subject of their mechanical properties.[9–13] However, an external heating such as a zone-heating is not able to heat the fiber evenly and instantaneously. The unequal heating induces a skin and core structure that inhibits production of the fiber with high modulus and high strength. To achieve a very

Correspondence to: A. Suzuki (a-suzuki@ab11.yamanashi.ac.jp).

Contract grant sponsor: Grant-in-Aid for Scientific Research (C) of Japan Society for the Promotion of Science.

Journal of Applied Polymer Science, Vol. 82, 2775–2783 (2001)

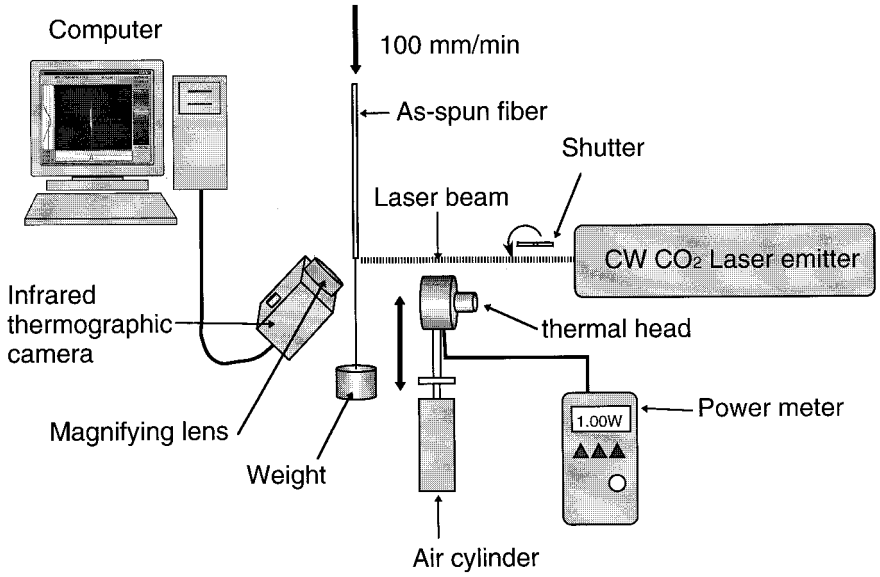

Figure 1 Scheme of apparatus used for laser-heating zone-drawing and laser-heating zone-annealing.

rapid heating and more uniform heating and to produce the high-performance fiber, a continuous-wave carbon dioxide (CW CO_2) laser was applied to the drawing and annealing of poly(ethylene terephthalate) (PET) fibers.

We present here the results pertaining to the mechanical properties and microstructure PET fibers zone-drawn and zone-annealed by the CW CO_2 laser.

EXPERIMENTAL

Material

The original material used in the present study was the as-spun PET fiber supplied by Toray Ltd. (Japan). The original fiber was a commercial grade fiber and had a diameter of about 0.25 mm, a degree of crystallinity of 4.5%, and a birefringence of 0.7×10^{-3}. The original fiber was amorphous and isotropic.

Apparatus for CW CO_2 Laser-Heating Zone-Drawing and Zone-Annealing

A schematic diagram of the apparatus used for the CO_2 laser-heating zone-drawing and zone-annealing is given in Figure 1. The apparatus consists of a CW CO_2 laser emitter (PIN10S, Onizuka Glass Co., Ltd., Japan), a power meter with a thermal head, a tensile testing machine (Orientec Co. Ltd., Japan), an air cylinder used to raise and lower the thermal head, an infrared thermographic camera (TH3101MR, NEC San-ei Instruments, Ltd., Japan) equipped with a magnifying lens, and a computer used to visualize data from the infrared thermographic camera. The CO_2 laser emitted light at 10.6 μm, and the laser beam was a 4.3-mm-diameter spot. Power density was measured by the power meter before the laser-heating.

One end of the as-spun monofilament was connected to a jaw equipped with crosshead of the tensile testing machine while the other is attached to a weight after passing through the two fixed pulleys. The fiber was fixed so that the center of the fiber axis coincided with that of laser beam. The laser beam was irradiated to the fiber and can be absorbed fully by the fiber. The fiber was moved downward at a speed of 100 mm/min, drawn, and annealed by irradiating the CW CO_2 laser ranging in beam power from 0.5 to 0.9 W.

Measurement

The draw ratio was determined in the usual way, by measuring the displacement of ink marks placed 10 mm apart on the fiber before drawing. The birefringence was measured with a polarizing microscope equipped with a Berek compensator (Olympus Optical Co., Ltd., Japan). The X-Z quartz compensator cut from a single crystal was additionally used because the highly oriented PET fiber had higher retardation. The density (ρ) of the fiber was measured at 23°C by a flotation technique using a carbon tetrachloride and toluene mixture. The degree of crystallinity, ex-

pressed as a weight fraction (X_w), was obtained by using the relation:

$$X_w = \{\rho_c(\rho - \rho_a)\}/\{\rho(\rho_c - \rho_a)\} \times 100 \quad (1)$$

where ρ_c and ρ_a are densities of crystalline and amorphous phases, respectively. In this measurement, a value of 1.455 g/cm^3 was assumed for ρ_c, and a value of 1.335 g/cm^3 was assumed for ρ_a.[14] The density of amorphous polymer was assumed to be constant, independent of treatments.

Equatorial and azimuthal wide-angle X-ray diffraction patterns for the fibers were obtained with a Rigaku X-ray generator and diffractometer equipped with a fiber specimen attachment (Rigaku Co., Japan). The X-ray unit was operated at 40 kV and 20 mA, and the radiation used was Ni-filtered CuKα.

Orientation factors of crystallites (f_c) were evaluated by using the Harmans equation[15]

$$f_c = \tfrac{1}{2}(3\langle\cos^2\phi_{c,Z}\rangle - 1) \quad (2)$$

where $\langle\cos^2\ \phi_{c,Z}\rangle$ represents the mean-square cosine of the angle (ϕ) between a c-crystal axis and a reference direction (Z) and can be calculated from eq. (3) induced by Wilchinsky method[16]:

$$\langle\cos^2\phi_{c,Z}\rangle = 1 - 2\langle\cos^2\phi_{010,Z}\rangle \quad (3)$$

which expresses the orientation of the c-axis with respect to the fiber axis as a function of the orientation of the (010) pole. The quantity $\langle\cos^2\ \phi_{010,Z}\rangle$ is determined from

$$\langle\cos^2\phi_{010,Z}\rangle = \frac{\int_0^{\pi/2} I(\phi)\sin\ \phi\cos^2\ \phi\ d\phi}{\int_0^{\pi/2} I(\phi)\sin\ \phi\ d\phi} \quad (4)$$

where

$$I(\phi) = \int_0^{\pi/2} I(\phi,\ \beta)\ d\beta \quad (5)$$

$I(\phi,\ \beta)$ is the pole-figure intensity. The method used to determine the f_c has been described in detail elsewhere.[17]

An amorphous orientation factor (f_a) was calculated by[18]

$$f_a = \frac{\Delta n - \Delta n_c^\circ f_c X_v}{\Delta n_a^\circ(1 - X_v)} \quad (6)$$

where X_v is the volume fraction crystallinity, $\Delta n_c{}^0$ an intrinsic crystallite birefringence, and $\Delta n_a{}^0$ is an intrinsic amorphous birefringence. The $\Delta n_c{}^0$ and the $\Delta n_a{}^0$ were taken to be 0.310 and 0.275.[19]

Wide-angle X-ray diffraction photographs of the fibers were taken by using a flat-film camera (Rigaku Co., Japan). The camera was attached to a Rigaku X-ray generator that was operated at 36 kV and 18 mA. The radiation used was Ni-filtered CuK_α. The sample-to-film distance was 40 mm. The fiber was exposed for 4 h to the X-ray beam from a pinhole collimator with a diameter of 0.4 mm.

FTIR spectra of the fibers were obtained at room temperature on a Perkin–Elmer *i*-Series FTIR microscope connected to a Perkin–Elmer Paragon 1000 spectrometer (Perkin-Elmer Co.). The spectra were measured at 4 cm^{-1} resolution and 64 scans.

Differential scanning calorimetry (DSC) measurements were carried out by using a Rigaku DSC 8230C calorimeter (Rigaku Co., Japan). The DSC scans were performed within the temperature range of 25 to 300°C, using a heating rate of 10°C/min. All DSC experiments were carried out under a nitrogen purge. The DSC instrument was calibrated with indium.

A Tensilon tensile testing machine (Orientec Co. Ltd., Japan) was used to determine tensile modulus, tensile strength, and elongation at break. A gauge length of 5 cm and elongation rate of 10 mm/min were used. The experimental results are the average of 10 measurements.

Dynamic viscoelastic properties were measured at 110 Hz with a dynamic viscoelastometer Vibron DDV-II (Orientec Co. Ltd., Japan). A 20 mm length of monofilament was needed between the two jaws. Measurements were carried out over a temperature range of 25 to about 220°C at an interval of 5°C. The average heating rate was 2°C/min.

RESULTS AND DISCUSSION

Optima Conditions for Laser-Heating Zone-Drawing and Laser-Heating Zone-Annealing

To determine the optimum condition of the laser-heating zone-drawing, the as-spun PET fiber was

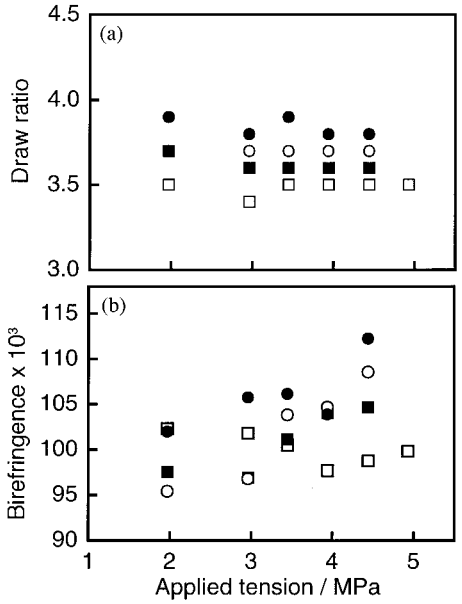

Figure 2 Changes in (a) the draw ratio and (b) the birefringence of the fibers zone-drawn at four different power densities (PD) with applied tension: (□) DP = 2.08 W cm^{-2}, (■) DP = 3.45 W cm^{-2}, (○) DP = 4.83 W cm^{-2}, (●) DP = 6.08 W cm^{-2}.

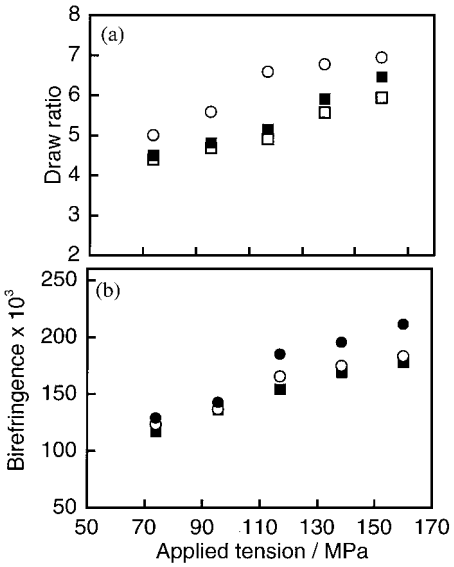

Figure 3 Changes in (a) the draw ratio and (b) the birefringence of the fibers zone-annealed at three different power densities (PD) with applied tension: (■) DP = 2.08 W cm^{-2}, (○) DP = 3.45 W cm^{-2}, (●) DP = 4.83 W cm^{-2}.

drawn under various conditions. A drawing speed used throughout the zone-drawing was 100 mm/min. The optimum drawing condition was determined by measuring the draw ratio and the birefringence of the fibers obtained under various conditions.

Figure 2(a,b) shows the changes in the draw ratio (λ) and the birefringence (Δn) of the fibers drawn at four different power densities (PD) with an applied tension (σ_a). The λ depends on the DP, but hardly on the σ_a. The Δn value tends to increase with increasing both the σ_a and the PD. The Δn of the fiber drawn under 4.44 MPa at PD = 6.08 W cm^{-2} shows a maximum value of 0.112. Consequently, this condition was chosen as the optimum for the laser-heating zone-drawing because the highest molecular orientation is achieved. The fiber zone-drawn under the optimum condition will hereinafter abbreviated the LH-ZD fiber.

Further, to optimize the condition of the laser-heating zone-annealing, the LH-ZD fibers were zone-annealed under various σ_a's and PDs. The laser-heating zone-annealing was carried out in three steps. The optimum condition for the first zone-annealing was determined by the λ, Δn, and tensile modulus (E).

Figure 3(a,b) shows the changes in the λ and the Δn of the annealed fibers with σ_a. The LH-ZD fibers were annealed at three different PDs. At all PDs, the λ and Δn increase by increasing the σ_a. The fiber annealed under 160 MPa at 4.83 W cm^{-2} has a maximum Δn of 0.211.

Figure 4 shows the E value plotted against the σ_a. The E value tends to increase with increasing the PD and the σ_a, but the E values of the fibers annealed at PD = 3.45 and 4.83 W cm^{-2} decrease in the annealing under σ_a = 160 MPa. Unlike the Δn value, the maximum E value in the first an-

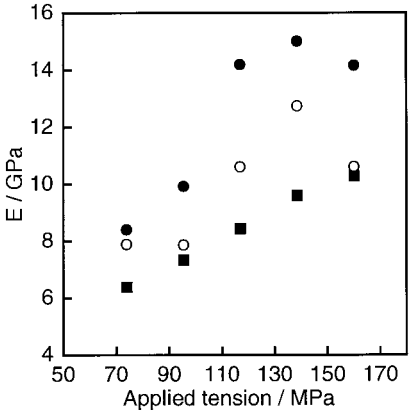

Figure 4 Changes in the tensile modulus of the fibers zone-annealed at three different power densities (PD) with applied tension: (■) DP = 2.08 W cm^{-2}, (○) DP = 3.45 W cm^{-2}, (●) DP = 4.83 W cm^{-2}.

Table I Optimum Conditions for the Laser-Heating Zone-Drawing and Zone-Annealing

Step	Applied Tension (MPa)	Power Density (W cm^{-2})	Maximum Surface Temperature of Fiber (°C)
Zone-drawing	4.44	6.08	164
1st zone-annealing	139	4.83	135
2nd zone-annealing	283	4.83	144
3rd zone-annealing	432	3.45	150

Table II Draw Ratio, Birefringence (Δn), Degree of Crystallinity (X_w), Crystallite Orientation Factor (f_c), and Amorphous Orientation Factor (f_a) for the Original Fiber and the Laser-Heated Zone-Drawn (LH-ZD) and Zone-Annealed (LH-ZA) Fibers

Fiber	Draw Ratio	$\Delta n \times 10^3$	X_w (%)	f_c	f_a
Original	—	0.70	4.5	—	—
LH-ZD	3.8	112	33	0.938	0.155
LH-ZA1	6.8	195	49	0.984	0.360
LH-ZA2	7.0	211	53	0.991	0.530
LH-ZA3	7.1	239	55	0.991	0.612

nealing is given by the treatment carried out at PD = 4.83 W cm^{-2} under 139 MPa. In the determination of the condition for the first zone-annealing, the result in Figure 4 is given priority over that in Figure 3. Therefore, the condition given the maximum E was chosen as the optimum one for the first laser-heating zone-annealing.

Further, the optima conditions for the second and the third laser-heating zone-annealing were also determined in the same way as in the case of the first zone-annealing. The fibers obtained by the first, second, and third zone-annealing under the optima conditions are designated as the LH-ZA1, LH-ZA2, and LH-ZA3 fiber, respectively.

The optima conditions for the laser-heating zone-drawing and zone-annealing, together with the maximum surface temperature measured using the infrared camera, are summarized in Table I. The superstructure and mechanical properties of the fiber obtained under each optimum condition will be discussed below.

It is difficult to measure the surface temperature of the fine fiber heated by irradiating the laser beam. However, the infrared thermographic camera equipped with the magnifying lens allows us to accurately measure the surface temperature of the fine fiber. Figure 5 shows the thermographies and temperature distributions parallel and

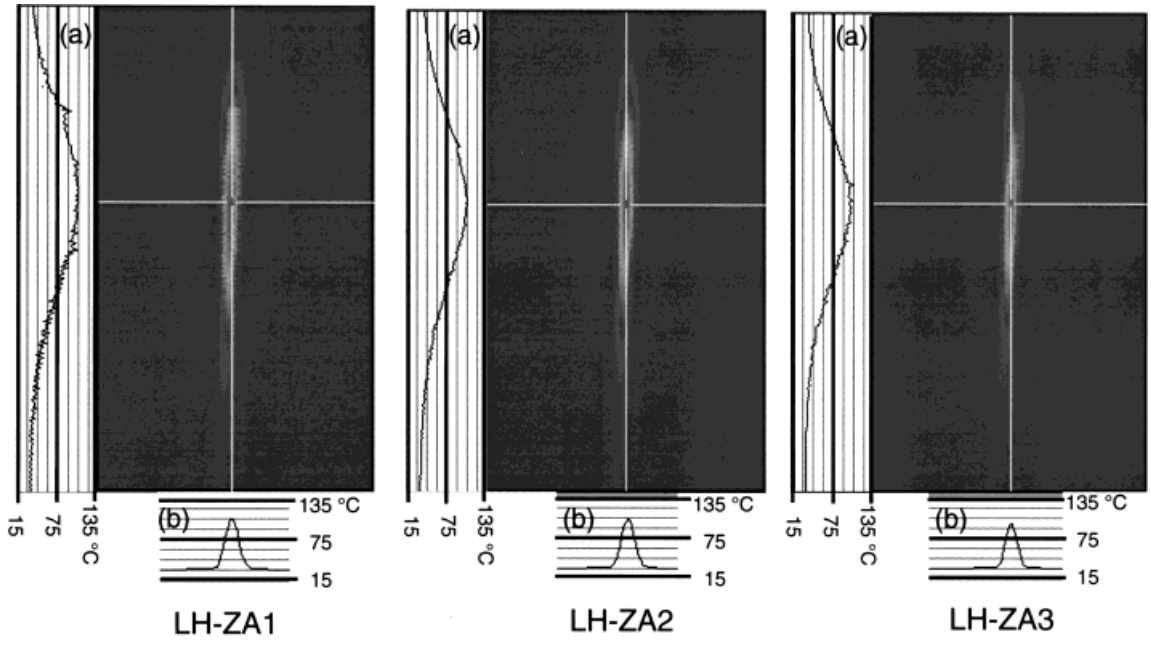

Figure 5 Thermographies and temperature distributions (a) parallel and (b) perpendicular to the fiber axis for the LH-ZA1, LH-ZA2, and LH-ZA3 fibers.

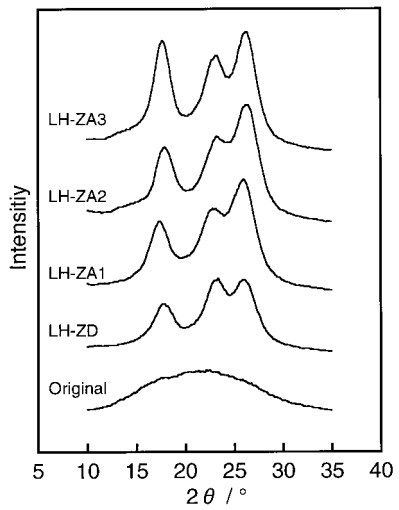

Figure 6 Equatorial wide-angle X-ray diffraction patterns of the original, LH-ZD, and LH-ZA fibers.

perpendicular to the fiber axis for the LH-ZA1, LH-ZA2, and LH-ZA3 fibers. The maximum surface temperature of the fiber was found to be in proportion to the laser power. As shown in Table I, the maximum temperature of the LH-ZA1 fiber irradiated at PD = 4.83 W cm^{-2} is 138°C, that of the LH-ZA2 fiber at PD = 4.83 W cm^{-2} is 144°C, and that of the LH-ZA3 fiber at PD = 3.45 W cm^{-2} is 150°C. The slight differences in the PD and the maximum temperature among the steps are attributable to a small deviation of the center of laser beam from the center of fiber. The infrared camera is able to exactly measure the surface temperature of the fiber heated by the laser beam.

Microstructure for the LH-ZD and LH-ZA Fibers

Table II lists the λ, Δn, X_w, f_c, and f_a for the LH-ZD and LH-ZA fibers. The λ and the Δn increase stepwise with the processing, and then the LH-ZA3 fiber obtained finally has $\lambda = 7.1$ and $\Delta n = 0.239$. The Δn value of the LH-ZA3 fiber is slightly lower than that of the zone-annealed fiber reported previously,[9] and it is almost the same value as the intrinsic crystallite birefringences ($\Delta n_c^0 = 0.22$–0.251) that were reported by a number of authors.[20–24]

The X_w also increases stepwise with the processing, and the LH-ZA3 fiber attains to $X_w = 55\%$. The additional crystallization due to the zone-annealing is presumably attributed to the increase in the number of crystallites and the crystal growth along the *c*-axis during the treatments. Peszkin et al.[25] reported on the basis of WAXD and SAXS results that the additional crystallization in the oriented fiber took place along the fiber axis of the already oriented crystal.

The f_c increases to 0.938 with only the laser-heating zone-drawing and further up to 0.991 with the laser-heating zone-annealing. The crystallites are easily aligned in the drawing direction. Murthy et al.[26] reported that the crystalline orientation increased rapidly at small draw ratios (< 3) and reached a plateau at higher draw ratios. On the other hand, the f_a increases from 0.155 for the LH-ZD fiber to 0.612 for the LH-ZA3 fiber. Unlike the f_c, the f_a is strongly dependent on the processing. The f_a closely related to the tensile modulus[12] as well as the X_w.

Figures 6 and 7 show the wide-angle X-ray diffraction photographs and equatorial patterns of the original, LH-ZD, and LH-ZA fibers. The equatorial and azimuthal breadths of three principal reflections (010, $\bar{1}10$, and 100) on the equator decrease with processing. The sharpening of three diffraction spots indicates an improvement in crystal perfection and an increase in the crystal size.

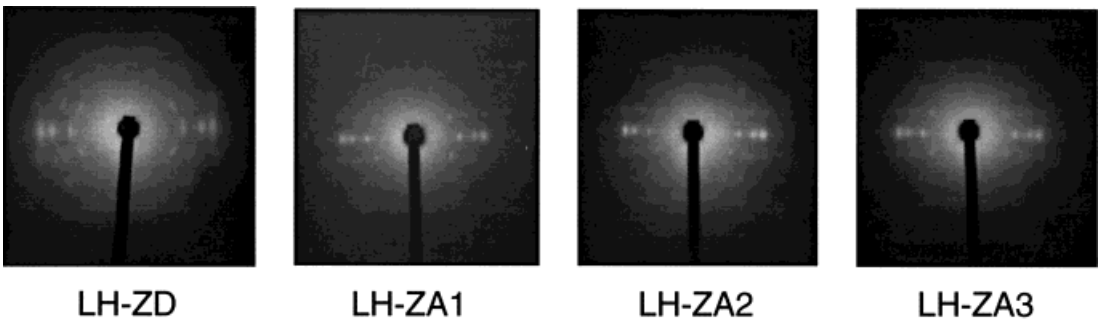

Figure 7 Wide-angle X-ray diffraction photographs of the original, LH-ZD, and LH-ZA fibers.

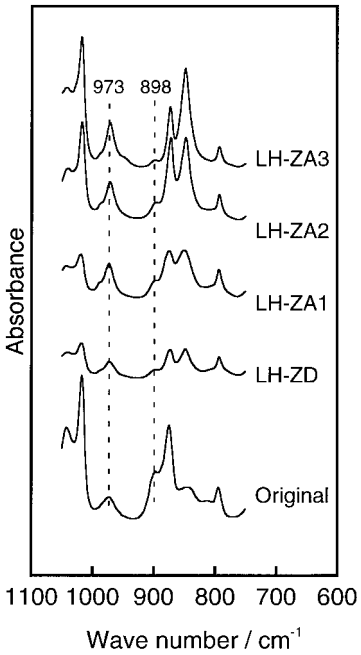

Figure 8 FTIR spectra of the original, LH-ZD, and LH-ZA fibers in the spectral range of 750-1050 cm^{-1}.

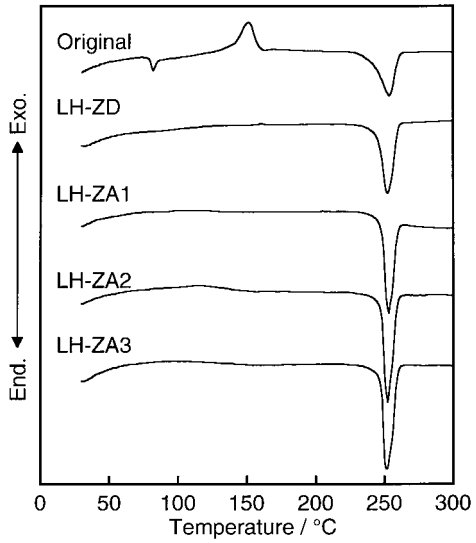

Figure 9 DSC curves of the original, LH-ZD, and LH-ZA fibers.

Figure 8 shows the FTIR spectra limited to the 750-1050 cm^{-1} for the original, LH-ZD, and LH-ZA fibers. To monitor conformational changes occurring in the polymer chains during the laser-heating, the bands situated at 973 and 898 cm^{-1} were used.[27–29] The former is attributed to a *trans* conformation, and the latter to a *gauche* conformation. The *trans* conformation can be involved in the crystalline and the amorphous phases, but the *gauche* conformation can be found only in the amorphous phase. The intensity of the bands situated at 973 cm^{-1} increases with the processing, but intensity of the bands situated at 898 cm^{-1} decreases. Therefore, the *trans* content increases with the processing, but the *gauche* decreases. The conformational changes can be ascribed to the development of the extended chain crystal and an extension of amorphous chains. The increment in the *trans* content related closely to the increases in the f_a and X_w, as described above.

Figure 9 shows DSC curves for the original, LH-ZD, and LH-ZA fibers. The original fiber shows a change in slope in the specific heat at 73°C, which corresponds to the glass transition; an exothermic transition at 150°C caused by a cold crystallization; and a broad melting endotherm peaking at 254°C. The LH-ZD and LH-ZA fibers have single melting-endotherm peaks at about 250°C. The difference in melting point between the original fiber and the treated fibers can be attributed to the morphological difference of crystallites; the lower melting peak was based on the fringed-micelle crystals formed by the strain-induced crystallization, and the higher one can be ascribed to the lamellar crystals which crystallized during the DSC scanning.[30] A sharpening of the melting peak with the processing is caused by an increase in the degree of perfection of the crystallites.[31,32]

Mechanical Properties for the LH-ZD and LH-ZA Fibers

Table III lists the tensile properties of the original, LH-ZD, and LH-ZA fibers. The tensile properties tend to increase stepwise with increasing processing. The maximum tensile modulus (19.8

Table III Tensile Properties for the Original Fiber, the Laser-Heated Zone-Drawn (LH-ZD), and Zone-Annealed (LH-ZA) Fibers

Fiber	Tensile Modulus (GPa)	Tensile Strength (GPa)	Elongation at Break (%)
Original	2.05	—	—
LH-ZD	6.31	0.53	62
LH-ZA1	15.0	1.02	7.9
LH-ZA2	18.1	1.35	7.4
LH-ZA3	19.8	1.21	6.9

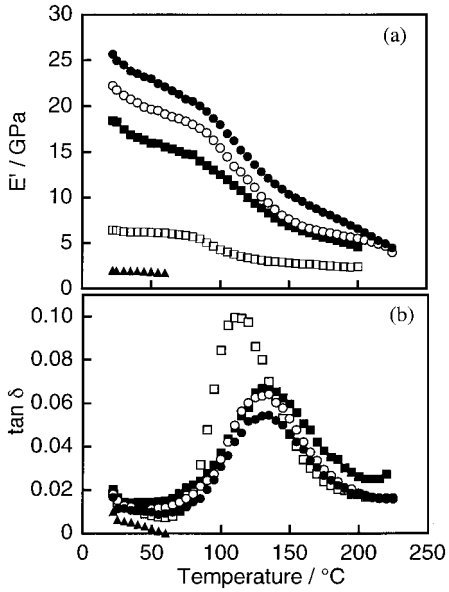

Figure 10 Temperature dependence of (a) storage modulus (E′) and (b) loss tangent (tan δ) for the original, LH-ZD, and LH-ZA fibers: (▲) original, (□) LH-ZD, (■) LH-ZA1, (○) LH-ZA2, (●) LH-ZA3.

GPa) is given at the LH-ZA3 fiber, and the maximum tensile strength (1.35 GPa) at the LH-ZA2 fiber. The improvement of tensile properties depends not only on the development of the amorphous orientation, but also on the increase in the crosslink density of the physical network made up of crystallites and molecular entanglements. These values are higher than those of the zone-annealed,[9] continuous zone-annealed[33] PET fibers, and that of the high-performance PET fiber produced by combination of threadline modification and postdrawing techniques.[34] However, there is still a considerable gap between the achieved and the theoretical modulus (110 GPa at room temperature[35]).

Figure 10(a,b) shows the temperature dependence of storage modulus (E') and loss tangent (tan δ) for the original, LH-ZD, and LH-ZA fibers. The E' values over a wide temperature range increase progressively with the processing. Finally, the E' value of the LH-ZA3 fiber reaches 25 GPa at 25°C. The E' values of all the fibers, except the original one, decrease monotonously with increasing temperature. The viscoelastic properties of the original fiber could not be measured above the T_g because fluidlike deformation caused slippage among the amorphous chains.

In the temperature dependence of tan δ [Fig. 10(b)], the LH-ZD and LH-ZA fibers show α peaks in the temperature range of 120–130°C, which are considered to originate from the glass transition. The α peak shifts to a higher temperature, decreases in its peak height, and becomes much broader with processing. The changes in position and profile of the α peak show that an increment in the degree of network density prevents the molecular mobility in the amorphous regions.

CONCLUSION

The laser-heating zone-drawing and laser-heating zone-annealing method was applied to PET fibers to improve their mechanical properties. The heating by the CW CO_2 laser was possible to draw and anneal the PET fiber and was found to be effective in producing the PET fibers with high modulus and high strength. The surface temperature of the fiber heated by the laser was obtained by using the infrared thermographic camera equipped with a magnifying lens.

We acknowledge the financial support of the Grant-in-Aid for Scientific Research (C) of Japan Society for the Promotion of Science. We are grateful to Toray Ltd. for supplying PET fibers.

REFERENCES

1. Zergioti, I.; Hatziapostolou, A.; Hontzopoulos, E.; Zervaki, A.; Haidemenopoulos, G. N. Thin Solid Films 1995, 271, 96.
2. Wang, J.; Wong, W. C. K. J Mater Process Technol 1999, 95, 164.
3. Hopfe, V.; Jäckel, R.; Schönfeld, K. Appl Surf Sci 1996, 106, 60.
4. Paiva, P.; Madelino, F.; Conde, O.; J Lumin 1999, 80, 141.
5. Panzner, M.; Wiedemann, G.; Henneberg, K.; Fischer, R.; Wittke, Th.; Dietsch, R. Appl Surf Sci 1998, 127–129, 787.
6. Hidouci, A.; Pelletier, J. M.; Ducoin, F.; Dezert, D.; El Guerjouma, R. Surf Coat Technol 2000, 123, 17.
7. Dadsetan, M.; Mirzadeh, H.; Shari, N. Radiat Phys Chem 1999, 56, 597.
8. Scarparo, M. A. F.; Chen, Q. J.; Miller, A. S.; Li, C. J.; Leary, H.; Allen, S. D. Appl Surf Sci 1996, 106, 275.
9. Kunugi, T.; Suzuki, A.; Hashimoto, M. J Appl Polym Sci 1981, 26, 1951.
10. Suzuki, A.; Kuwabara, T.; Kunugi, T. Polymer 1998, 39, 4235.
11. Suzuki, A.; Kohno, T.; Kunugi, T. J Polym Sci, Polym Phys Ed 1998, 36, 1731.

12. Suzuki, A.; Chen, Y.; Kunugi, T. Polymer 1998, 39, 5335.
13. Suzuki, A.; Toda, K.; Kunugi, T. Polymer 2000, 41, 6061.
14. Danderg, R. R.; Bunn, C. W. Proc R Soc London, Ser A 1954, 226, 531.
15. Harmans, P. H.; Platzek, P. Kolloid Z 1939, 88, 68.
16. Wilchinsky, Z. W. J Appl Phys 1963, 30, 792.
17. Alexander, L. E. Diffraction Methods in Polymer Science; Wiley-Interscience: New York,1969; Chapter 4, pp 241–252.
18. Stein, R. S.; Norris, F. H. J Polym Sci 1956, 21, 381.
19. Gupta, V. B.; Sett, S.. K.; Deorukhkar, D. D. Polymer 1989, 30, 341.
20. Patterson, D.; Ward, I. M. Trans Faraday Soc 1957, 53, 1516.
21. Dumbleton, J. H. J Polym Sci, Part A: Polym Chem 1968, 6, 795.
22. Konda, A.; Nose, K.; Ishikawa, H. J Polym Sci, Part A: Polym Chem 1976, 14, 1495.
23. Kunugi, T.; Shiratori, K.; Uematu, K.; Hashimoto, M. Polymer 1979, 20, 171.
24. Garg, S. K. J Appl Polym Sci 1982, 27, 2857.
25. Peszkin, P. N.; Schultz, J.M.; Lin, J. S. J Polym Sci, Polym Phys Ed 1986, 24, 2592.
26. Murthy, N. S.; Bray, R. G.; Correale, S. T.; Moore, R. A. F. Polymer 1995, 36, 3863.
27. Lin, S. B.; Koenig, J. L. J Polym Sci, Polym Phys Ed 1982, 20, 2277.
28. Yazdanian, M.; Ward, I. M.; Brody, H. Polymer 1985, 26, 1779.
29. Quintanilla, L.; Rodríguez-Cabello, J. C.; Jawhari, T.; Pastor, J. M. Polymer 1993, 34, 3787.
30. Elenga, R.; Seguela, R.; Riestsch, F. Polymer 1991, 32, 1975.
31. Wills, A. J.; Capaccio, G.; Ward, I. M. J Polym Sci, Polym Phys Ed 1980, 18, 493.
32. Gaymans, R. J.; Van Utteren, T. E. C.; Van Der Berg, J. W. A.; Schuyer, J. J Polym Sci, Polym Chem Ed 1977, 15, 537.
33. Suzuki, A.; Sato, Y.; Kunugi, T. J Polym Sci, Polym Phys Ed 1998, 36, 473.
34. Wu, G.; Tucker, P. A.; Cuculo, J. A. Polymer 1997, 38, 1091.
35. Thistlethwaite, T.; Jakeways, R.; Ward, I. M. Polymer 1988, 29, 61.